Copyright 2022 Society of Photo-Optical Instrumentation Engineers. One print or electronic copy may be made for personal use only. Systematic reproduction and distribution, duplication of any material in this paper for a fee or for commercial purposes, or modification of the content of the paper are prohibited.
Roberto Fallica, Danilo De Simone, Steven Chen, Muhammad Safdar, Hyo Seon Suh, "Scaling and readiness of underlayers for high-numerical aperture extreme ultraviolet lithography," J. Micro/Nanopattern. Mats. Metro. 21(4) 044601 (15 November 2022) https://doi.org/10.1117/1.JMM.21.4.044601

Scaling and readiness of underlayers for high-numerical aperture extreme ultraviolet lithography

Roberto Fallica,[a,*] Danilo De Simone,[a] Steven Chen,[a,b] Muhammad Safdar,[a,c] and Hyo Seon Suh[a]
[a]IMEC, Leuven, Belgium
[b]Karlsruhe Institute of Technology (KIT), Karlsruhe, Germany
[c]Munich University of Applied Sciences (MUAS), Munich, Germany

Abstract. With the introduction of high-numerical aperture (NA) extreme ultraviolet (EUV) lithography, the thickness of layers in the lithographic stack will scale owing to reduced depth of focus and etch budget. The consequence of thinning down underlayers for EUV lithography has been scarcely investigated. In here, we assessed the readiness of nine state-of-the-art underlayers, spin-on and dry deposited, in thickness series down to 4 nm nominal. Preliminarily, the coating quality of these underlayers was evaluated. Thickness uniformity across 300 mm wafer ranged from about ± 0.5 nm to $< \pm 0.05$ nm depending on the coating technique employed. Surface roughness of the underlayers varied from as much as 0.63 nm to as low as 0.062 nm but was not impacted by thickness scaling. Film density and total surface energy varied by <10% with thickness. EUV lithography of dense lines/spaces arrays of pitch 28 nm was carried out using a positive tone chemically amplified photoresist. Dose-to-size and exposure latitude changed by $< \pm 5\%$ when thickness of underlayer was decreased. Failure free process was at most 1 nm smaller for thinner underlayer than it was for the thinnest version of each type. The unbiased linewidth roughness increased consistently but limitedly (<5%) when thinner underlayers were used, mainly due to a reduction in the correlation length. By calculating the power spectral density of the blanket underlayer we can pinpoint this effect to a reduction of correlation length of the underlayer own surface roughness. Finally, Z-factor calculations demonstrated that overall photoresist performance depended more significantly on the specific underlayer type ($\pm 12.6\%$) than it did on underlayer thickness ($\pm 8\%$). All these results indicate that most of underlayers investigated had limited impact on the properties as well as the patterning performance when scaling in view of high NA EUV. © *2022 Society of Photo-Optical Instrumentation Engineers (SPIE)* [DOI: 10.1117/1.JMM.21.4.044601]

Keywords: extreme ultraviolet; extreme ultraviolet lithography; high-numerical aperture; underlayer; photoresist; scaling; numerical aperture; lithography.

Paper 22057G received Sep. 14, 2022; accepted for publication Oct. 26, 2022; published online Nov. 15, 2022.

1 Introduction

Extreme ultraviolet (EUV) lithography, the next-generation optical lithography technology that uses light at 13.5 nm wavelength, has reached maturity and is being adopted for high-volume manufacturing of semiconductor devices worldwide.[1] Currently, commercial EUV scanner models NXE3xxx are equipped with 0.33 numerical aperture (NA) optics that can pattern dense lines/spaces arrays to a resolution of pitch 28 nm. To push forward the resolution toward the next technology nodes and reach 20 nm pitch resolution and beyond, a new generation of scanners (EXE5xxx) featuring 0.55 NA is being developed.[2] High-NA EUV will enable further scaling of integrated circuits by ensuring that the normalized image log-slope (NILS), a metric for the quality of the aerial image,[3] remains at acceptable levels to pattern devices at technology node "2.1 nm" and beyond.[4]

*Address all correspondence to Roberto Fallica, roberto.fallica@imec.be, imec-int.com

1932-5150/2022/$28.00 © 2022 SPIE

Downloaded From: https://www.spiedigitallibrary.org/journals/Journal-of-Micro/Nanopatterning,-Materials,-and-Metrology on 25 May 2023
Terms of Use: https://www.spiedigitallibrary.org/terms-of-use

From the materials standpoint, photoresists for EUV are expected to fulfill a multitude of requirements such as high resolution, high sensitivity, low sidewall roughness, low defectivity, thermodynamic stability, high chemical uniformity, and others.[5] The introduction of high-NA EUV will exacerbate these requirements for two reasons. First, the optical depth of focus (DOF) is going to shrink with the reciprocal of the square of NA according to the well-known equation: $\mathrm{DOF} = k_2 \frac{\lambda}{\mathrm{NA}^2}$. As a result, the available DOF of a high-NA EUV system will only be about 36% of that of a 0.33 NA scanner, all other parameters being equal. In practice, available depth of focus might reduce from ∼150[6] to ∼50 nm thus demanding photoresist thickness reduction (although recent experiments carried out at pseudo-0.5 NA EUV tool showed that the impact might be marginal for contact hole patterning[7]).

The second issue is the need for isotropic scaling in order to maintain a constant aspect ratio when pitch shrinks. This problem is not specific to high-NA EUV: when pitch shrinks, aspect ratio of photoresist patterns increases which in turn leads to higher collapse probability during development and rinse.[8] To mitigate pattern collapse, photoresists for high-NA EUV will have to be thinner than those used today with detrimental consequences on the local critical dimension uniformity, line edge/width roughness (LER/LWR), process window,[9] and on signal-to-noise ratio of scanning electron microscopy (SEM) image acquisition[10] and data extraction.[11] Consequently, great effort is being put into investigating and predicting thin photoresist films performance ahead of high-NA EUV. A variety of new approaches such as etch-litho synergy,[9] preprocessing and postprocessing holistic approach,[12] photoresist-underlayer matching,[8] complementary direct self-assembly,[13] and others, are being taken to this purpose.

Meanwhile, it should not be overlooked that underlayers (a.k.a. hardmasks) also have to scale in thickness due to etching budget considerations. Take for instance the positive-tone chemically amplified resists (CAR), typically between 35 and 45 nm thick, used nowadays for pitch 32 nm lines/spaces patterning: several technology nodes ahead, the 16 nm pitch lines/space will have to use 20 nm thick photoresists to maintain the same aspect ratio as today. Underlayers will arguably have to shrink at a comparable rate, from 10 nm of today to 4 or 3 nm foreseen in technology node "2.1 nm" (under the assumption that etch selectivity of photoresist versus underlayer remains the same). These estimates lead to the qualitative scaling roadmap shown in Fig. 1.

Despite these considerations, the scaling effects on EUV underlayers have not been explored as extensively as those on photoresists. A number of physical and chemical properties of thin films have been demonstrated to vary with thickness at the nanoscale, such as glass transition temperature,[14] elastic modulus,[15] surface roughness,[16,17] correlation length,[17] Hurst's exponent,[16] refractive index,[18] and radius of gyration,[19] as well as theoretically.[20] Any such change is

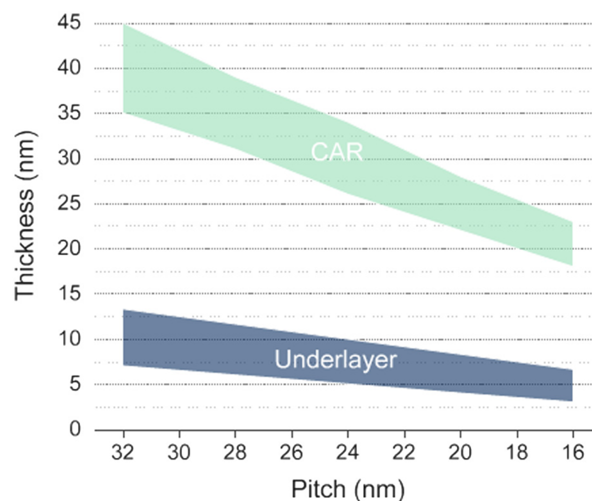

Fig. 1 A qualitative roadmap of photoresists and underlayers thickness scaling in EUV lithography. For photoresist we consider here only positive-tone CAR. Photoresist thickness ranges between 35 and 45 nm at pitch 32 nm lines/spaces patterning and, for pattern collapse reasons, is expected to shrink to 20 nm in future technology nodes. The underlayer thickness is typically 10 nm as of today and is expected to follow a comparable scaling trend.

Downloaded From: https://www.spiedigitallibrary.org/journals/Journal-of-Micro/Nanopatterning,-Materials,-and-Metrology on 25 May 2023
Terms of Use: https://www.spiedigitallibrary.org/terms-of-use

evidently undesirable from lithographic process control standpoint and is relevant for EUV lithography as witnessed by early works that studied the glass transition temperature as a function of thickness,[21] and recent characterization of EUV underlayers scaled down to 5 nm.[22]

For all these reasons, in this work we evaluated the readiness of underlayer scaling for high-NA EUV lithography from the point of view of their physical properties and impact on patterning quality. In collaboration with external materials suppliers, we had the opportunity to characterize nine underlayer samples in thickness series down to 4 nm (nominal thickness) so as to replicate the process conditions foreseen in future technology nodes. In the first part of this work, we report out the characterization of blanket films to assess whether the integrity of ultrathin underlayers could be compromised when thinning down. Potential roadblocks include thickness uniformity, density fluctuations, and uneven coverage. In the second part, we look at the lithographic impact of thinning underlayers by EUV patterning of a state-of-art CAR. Finally, we use lithographic figures of merit to draw conclusions on the readiness and relative impact of underlayers on EUV photoresist patterning in general.

2 Samples Description and Experimental Details

2.1 *Samples Description: the Photoresist and the Underlayers*

In this study, four materials suppliers provided nine underlayers (UL) and one CAR, all specifically designed for EUV lithography. The nine underlayers' chemistry varied and included siloxanes, polycarbosilanes, silicon oxycarbide glasses, and others. An organic underlayer (B) was also measured as benchmark. The CAR, positive tone organic resist, 30 nm thick was preliminarily qualified for pitch 28 nm EUV patterning capability on a reference underlayer (data not reported). Spin-coated samples were prepared in 300 mm track; deposited samples were prepared in proprietary 300 mm-scale deposition tools. Materials suppliers were required to provide underlayers in series of at least two thickness versions each, with a target of 5 to 3 nm minimum nominal thickness. There was no other specific requirement for the underlayer typology. Notably, materials suppliers were also informed that the photoresist of choice was organic CAR, and it was intended that the underlayer should be suited and optimized for this specific case. Care was taken to follow the manufacturers' specifications to maximize the quality and yield of the samples. The underlayers were coated or deposited directly on top of bare silicon wafers of 300 mm diameter and 775 μm thickness. These wafers typically have a native Si oxide layer. The underlayers' code names and nominal thickness are summarized in Table 1.

Table 1 Samples description: underlayer code names and their nominal thickness, and photoresist used and its thickness.

Underlayer code name	Thickness, nominal (nm)
A	8, 6, 4
B	20, 5
C	8, 6, 4
D	8, 6, 4
E	8, 6, 4
F	8, 6, 4
G	8, 6, 4
H	8, 6, 4
L	10, 5
Photoresist	**Thickness, nominal (nm)**
Positive tone CAR	30

Downloaded From: https://www.spiedigitallibrary.org/journals/Journal-of-Micro/Nanopatterning,-Materials,-and-Metrology on 25 May 2023
Terms of Use: https://www.spiedigitallibrary.org/terms-of-use

2.2 *Physical Characterization Methods*

Experimental characterization was carried out on blanket underlayer films (unpatterned and not covered with photoresist) to validate actual thickness, thickness uniformity across 300 mm wafer, and surface roughness. To get an as accurate as possible measurement of the actual thickness of the ultrathin underlayer samples, X-ray reflectivity was used (Cu Kα source, 0.154 nm wavelength). A 300 mm scale spectroscopic ellipsometer in the wavelength range 215 to 800 nm was used to determine the variation of the film thickness across 21 measurement locations on wafer. Together, these two techniques are complementary. It should be noted that native silicon oxide layer (between 1 and 2 nm thick)[23,24] is ubiquitously present on bare <100> Si surface and is a source of measurement error especially when the underlayer also contains Si, O, or Si-O bonds.

Surface roughness of underlayers was measured by inline atomic force microscopy (AFM) in tapping mode, over two locations at the wafer center and wafer edge. Scan area was 1000^2 nm^2 with resolution of 4 nm/pixel, automatically corrected for tilt and bow artifacts by the tool. Surface roughness values are reported in root mean square (R_q). AFM can point to possible issues such as intra-wafer center-to-edge nonuniformity. Besides, it is not unusual that films show increasingly higher roughness when scaled towards single nanometer thickness: in such cases, AFM can detect uneven coverage of the substrate.[16,17] The power spectral density of the surface roughness was calculated using a discrete fast Fourier transform algorithm[25] on the scan height data.

Density of thin films is another quantity that should be unchanged when scaling thickness for etch selectivity reasons. To assess film density, the weight of 300 mm wafers was measured by microbalance measurement before and after the preparation of each underlayer. The weight difference, including the instrumental uncertainty, was plotted against the film volume (calculated by considering the wafer area minus a cleaned edge of 3 mm, and the actual thickness measured in the previous step). A slope of the linear fit to the data (with intercept constrained to the origin of axis) yielded the average density of each underlayer and the standard deviation. The latter represents density variations among underlayers of the same type when prepared to different thicknesses.

Surface energy of blanket underlayer films was measured using the sessile drop method of two liquids (water and diiodomethane) as detailed elsewhere.[26] Both polar and nonpolar surface energy components were extracted. In the following, only the total surface energy (sum of these two components) is reported.

2.3 *EUV Lithography*

Assessment of thin underlayers' impact on CAR lithography was performed using ASML's NXE3400B EUV scanner located at IMEC (Leuven, Belgium) premises. An EUV reticle featuring dense vertical lines/spaces arrays of pitch 28 nm and nominal 1:1 ratio was used to pattern the wafer in a focus-exposure-matrix (FEM) fashion. The center dose of the FEM wafers was 67 mJ/cm^2, the dose step was 1.5 mJ/cm^2, the center focus was 0.000 μm, and the focus step was 0.020 μm. The EUV illuminator was a customized X dipole specifically optimized for pitch 28 nm dense vertical lines/spaces.

2.4 *CDSEM Inspection after Lithography and Computational Metrology*

Photoresist samples were inspected after EUV exposure and development by critical dimension scanning electron microscope (CDSEM) with field of view of 0.82^2 μm^2 and 0.8 nm/pixel resolution. Lines' critical dimension (CD) measured on focus-exposure matrix wafers were used to calculate dose-to-size (at CD = pitch/2), best focus, and elliptical exposure latitude (as CD = pitch/2 $\pm$ 10%). For each wafer, the chip that was closest to the calculated dose-to-size and best focus was then inspected in depth by taking 50 CDSEM images with field of view 1.6^2 μm^2 and 0.8 nm/pixel resolution according to previously defined protocol.[27] These 50 images were analyzed as a batch using FRACTILIA's MetroLER software (v. 2.8.5)[28] to determine unbiased line width roughness (LWR), unbiased line edge roughness (LER), power spectral density (PSD), correlation length, and PSD(0), according to well-established methodology.[29]

Downloaded From: https://www.spiedigitallibrary.org/journals/Journal-of-Micro/Nanopatterning,-Materials,-and-Metrology on 25 May 2023
Terms of Use: https://www.spiedigitallibrary.org/terms-of-use

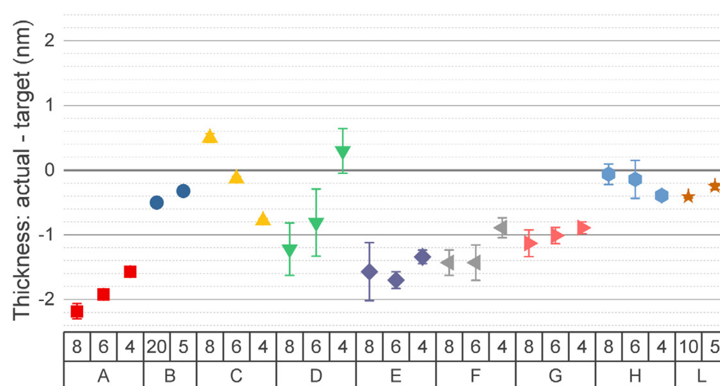

Fig. 2 Difference between actual thickness and target thickness, in nm, of the blanket underlayers. In the *X*-axis, letters are code names for underlayers; numbers indicate the target nominal thickness. Symbols represent thickness measured by XRR; error bars indicate coating uniformity across 21 locations on a 300 mm wafer by ellipsometry.

3 Results

3.1 *Quality of Blanket Scaled Underlayers*

Initial assessment of underlayer quality involved the characterization of the blanket films to determine the materials' coverage of the wafer. The actual measured underlayer thickness (symbols in Fig. 2) was in most cases below target by about 1 nm and occasionally, such as underlayers (A), as much as 2 nm below target. Some underlayers (E, F, G) showed an approximately constant offset with respect to the target thickness which might be ascribed to a systematic measurement error due to the presence of native silicon oxide. In one case, thickness accuracy was better in the thinner version than it was for the thicker, which led to a narrower thickness range (D). In another case (C), this trend was reversed, which led to a broader thickness spread. The thickness uniformity, across 21 measurement locations on the 300 mm wafer, is reported as the error bar in Fig. 2. Uniformity varied greatly from high (A, L) to low (D) and is ascribed to underlayer preparation methods, which included manual coating by pipette, coating from small volume dispenser units, track coating from gallon supply, and dry deposition. It should be noted that thickness targeting was not the main scope of this work and does not invalidate our methodology, as long as samples with well-defined thickness series can be accurately obtained.

Regarding the surface roughness, photoresists and underlayers for EUV lithography typically have R_q below 1 nm, comparably lower than inorganic crystalline films. Although there is no specific requirement for surface roughness of EUV materials, it is reasonable to expect R_q to be <10% of film thickness. The measured root mean square (RMS) surface roughness of samples is summarized in Fig. 3 and ranged greatly from as much as 0.63 nm to as low as 0.062 nm. In most cases, the roughness was not impacted by the thickness scaling. Only one type of sample (A) showed high roughness in absolute values, and up to +55% increase when thinning from 8 to 4 nominal thickness, an effect which might be due to the lowest absolute thickness value of these samples (reported in Fig. 2). Other samples only showed a slight increase (B, C, D,) or even reduction of roughness when scaling. These results show that underlayers, including those based on polymeric spin-on precursors, are capable of forming very thin layers despite approaching a scale comparable to the polymer's own radius of gyration[16,17] a phenomenon that is known to cause, for instance, anisotropy in the molecular arrangement;[19,30] and of exacerbating the existing topography in the case of nonconformal dry deposited thin films.[31] The lack of such effects is a good proof of scalability for high-NA application.

The density of the underlayers varied greatly from 1.1 to 1.85 g/cm^3 due to the different chemistries and preparation methods. In comparison, typical EUV photoresist have density of 1.2 g/cm^3. Figure 4 shows the average density of each underlayer, as well as the fluctuations in density among samples of different thicknesses (error bars). For most samples, the density was unaffected by scaling. In other cases (A, D, E, and F) density fluctuations were more marked when thickness changed, which might impact the etch resistance.

Downloaded From: https://www.spiedigitallibrary.org/journals/Journal-of-Micro/Nanopatterning,-Materials,-and-Metrology on 25 May 2023
Terms of Use: https://www.spiedigitallibrary.org/terms-of-use

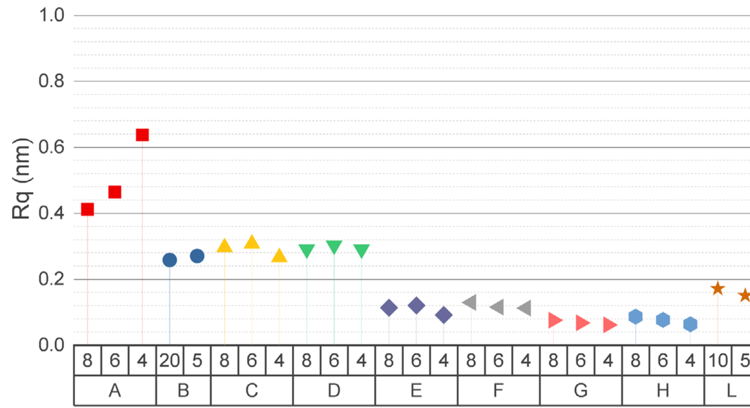

Fig. 3 The RMS surface roughness of scaled underlayers shows the impact of thinning. In the *x*-axis, letters are code names for underlayers; numbers indicate the target nominal thickness. Most of underlayers demonstrated to be scalable in thickness with no detrimental consequences on the surface roughness.

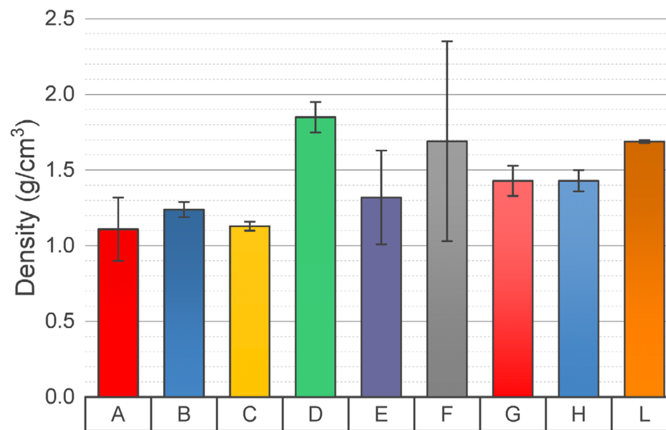

Fig. 4 Average density of underlayers (bar height) and fluctuations among samples of different thickness (error bars). Larger error bars indicate greater density fluctuations when the thickness of a given underlayer is scaled.

The total surface energy of blanket underlayers is reported in relative terms, normalized to the thickest version of each type, in Fig. 5. The data show that the surface energy fluctuates with thickness by <8% within each underlayer type. As a result, surface energy of underlayers was impacted minimally by thickness scaling with beneficial effects on the adhesion and collapse of photoresist.[8] Previous studies on polymers have reported that the surface energy depends in a non-linear way on the thickness, owing to the anisotropy of the in-plane versus out-of-plane radii of gyration:[19] however, we did not detect such an effect in this work.

3.2 *EUV Lithography Performance on Scaled Underlayers*

In this section, we review the impact of reducing underlayer thickness on the lithographic performance of a CAR. Dose-to-size, depth of focus, exposure latitude, linewidth roughness, failure free process window, and Z-factor[32] are the key performance indicators used. To focus on the relative variations of the key parameters with thickness, all data reported here was normalized to the thickest layer of each underlayer type.

The CDSEM images of CAR patterned on the nine underlayers in thickness series, 25 samples in total, taken at the chip closest to dose-to-size and best focus of the FEM wafer, are shown in Fig. 6. It can be noted that image contrast varies among these samples, something we mainly ascribe to different secondary electron yield of each underlayer type. Within each thickness

Downloaded From: https://www.spiedigitallibrary.org/journals/Journal-of-Micro/Nanopatterning,-Materials,-and-Metrology on 25 May 2023
Terms of Use: https://www.spiedigitallibrary.org/terms-of-use

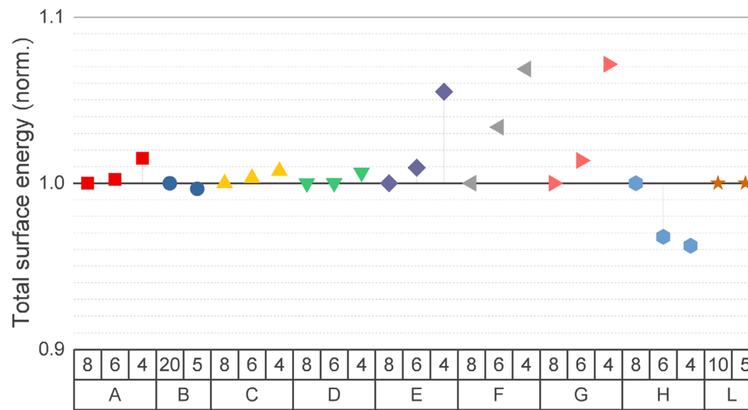

Fig. 5 Total surface energy dependence on the underlayer thickness, normalized to the thickest version of each underlayer type. The effect is limited to <8% variation within each underlayer type.

series, contrast also changes, although to a lesser extent than it has been reported in the case of thin photoresist films.[10] CAR patterning does not show any problem at the dose-to-size and best focus when used in conjunction with most of these underlayers. One underlayer (H) showed mediocre adhesion and pattern collapse possibly due to mismatching surface energy with photoresist. Adhesion of (H) seemed to improve when thinner version was used (H4), for reasons that are unclear.

The relative effect of underlayer thickness on dose-to-size is summarized in Fig. 7, where data is again normalized to the dose-to-size of the thickest layer of each type. The effect of underlayer thickness on dose-to-size was $< \pm 3\%$, which is nearly within experimental and reproducibility error. Similar considerations could be done for the exposure latitude, calculated by elliptical process window, and shown in relative terms in Fig. 8. EL was minimally impacted by thickness scaling ($< \pm 5\%$) for most of the samples, with the exception of (C) which had an EL reduction of -12% at worst.

The failure-free process window was evaluated by analyzing patterning defects across all CD range available on the FEM wafer. The minimum line CD without pattern collapse or breaks and the maximum line CD without bridge defects is shown in the bar plot of Fig. 9. Some samples showed a sizeable reduction of the failure-free window (A and B) when thickness of underlayer was reduced. Other samples (C, D, F, G, and L) had negligible variations. In one case (E), failure-free process window seemed to increase marginally (possibly an artifact due to the limited line CDs available on FEM wafer). Data also showed that underlayer type overwhelm thickness effects: e.g., the sample that resulted in abundant pattern collapse (H) seen in Fig. 6, did so irrespective of thickness.

The total unbiased LWR of CAR patterned on top of different scaled underlayers is summarized in Fig. 10(a). The general trend shows an increase in unbiased LWR when thinning the underlayers, irrespective of the specific type of underlayer. Note that the sample H was affected by abundant pattern collapse and the normalization led to artifact due to the high total LWR (>8 nm): no conclusion can be made. For all other samples, it can be also noted that there was no correlation between the LWR and the surface roughness of the underlayers, previously shown in Fig. 3: for instance, high surface roughness (A) did not cause substantial LWR worsening. Similar considerations hold valid for the unbiased LER, shown in Fig. 10(b).

To understand the increase of total LWR when underlayers were thinned down, we decomposed the LWR into its zero-frequency component, PSD(0), and its correlation length using power spectral density analysis. The PSD(0), shown in Fig. 10(c), varied within $\pm 5\%$ for within each underlayer and showed no correlation with thickness. Instead, the LWR correlation length [Fig. 10(d)] consistently decreased with thickness for all underlayer types by an amount ranging from -5% to -10%. This observation leads to the conclusion that the increase in total LWR was driven by the increase in high-frequency linewidth roughness.

We also observed that the correlation length of LWR was not related to the surface roughness of the blanket underlayers (Fig. 3). Instead, the decrease of the LWR correlation length might had

Downloaded From: https://www.spiedigitallibrary.org/journals/Journal-of-Micro/Nanopatterning,-Materials,-and-Metrology on 25 May 2023
Terms of Use: https://www.spiedigitallibrary.org/terms-of-use

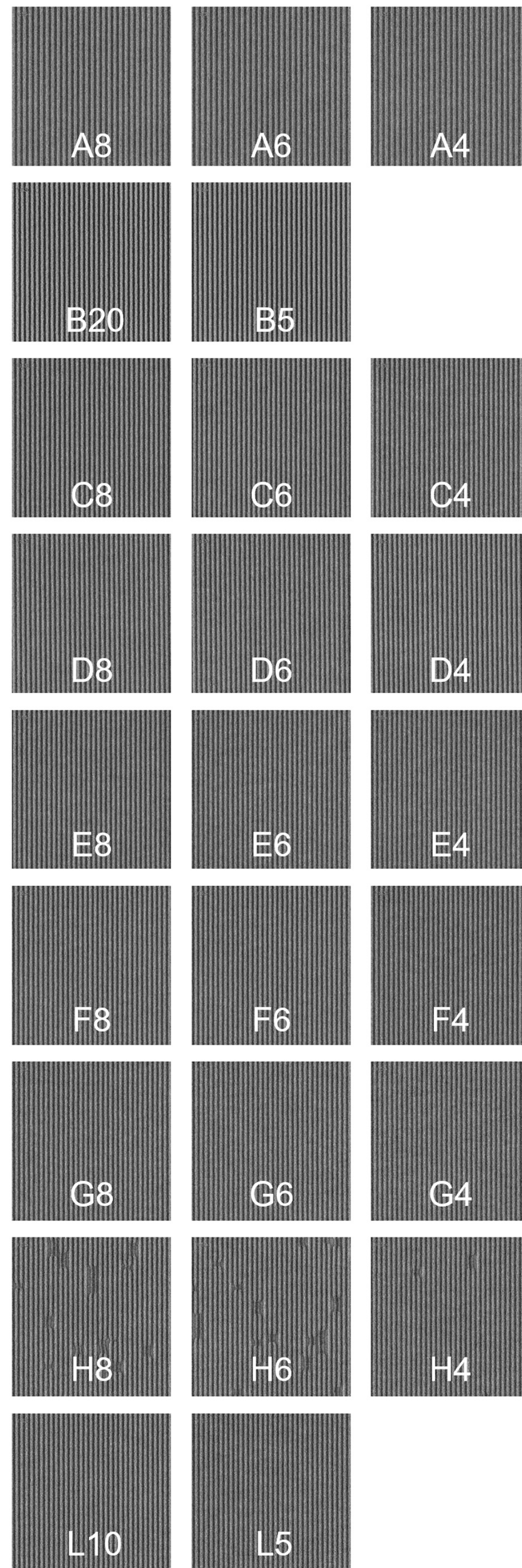

Fig. 6 CDSEM images of CAR lines/spaces patterns of pitch 28 nm, printed on nine underlayers of decreasing thickness. The letter indicates the underlayer sample, and the number indicates the nominal underlayer thickness, in nm.

Downloaded From: https://www.spiedigitallibrary.org/journals/Journal-of-Micro/Nanopatterning,-Materials,-and-Metrology on 25 May 2023
Terms of Use: https://www.spiedigitallibrary.org/terms-of-use

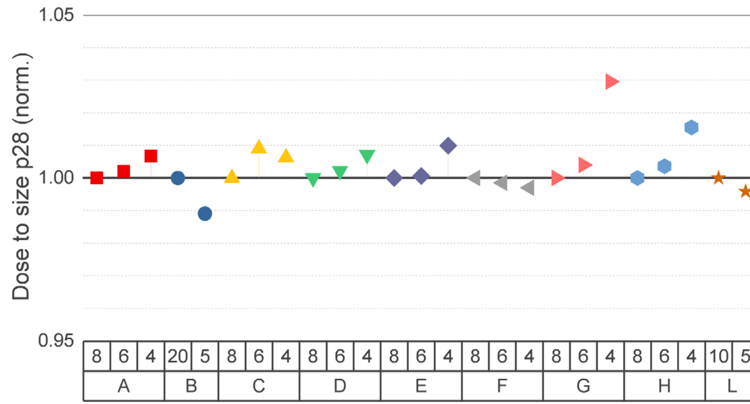

Fig. 7 Dose-to-size of a CAR, pitch 28 nm lines/spaces, patterned by EUV on top of nine different underlayers of decreasing thickness. Values are normalized to the dose-to-size of the thickest film of each type. Effect of underlayer thickness on dose-to-size was below ±3%.

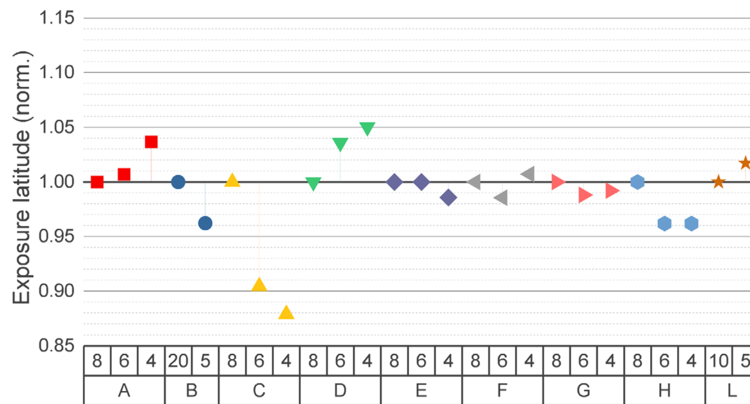

Fig. 8 Exposure latitude of a CAR, pitch 28 nm lines/spaces, patterned by EUV on top of nine different underlayers of decreasing thickness and calculated by elliptical process window. Values are normalized to the exposure latitude of the thickest film of each type. Effect of underlayer thickness on exposure latitude was below ±5% for most underlayers.

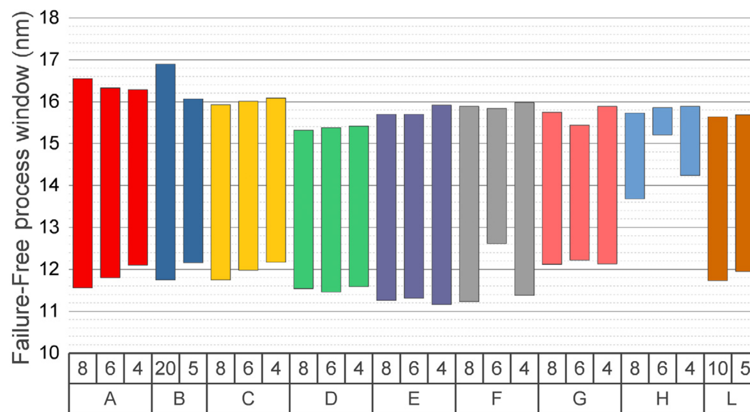

Fig. 9 Failure-free process window a CAR, pitch 28 nm lines/spaces, patterned by EUV on top of nine different underlayers of decreasing thickness. The bars represent the range between minimum line CD without pattern collapse and maximum CD without bridge defects.

Downloaded From: https://www.spiedigitallibrary.org/journals/Journal-of-Micro/Nanopatterning,-Materials,-and-Metrology on 25 May 2023
Terms of Use: https://www.spiedigitallibrary.org/terms-of-use

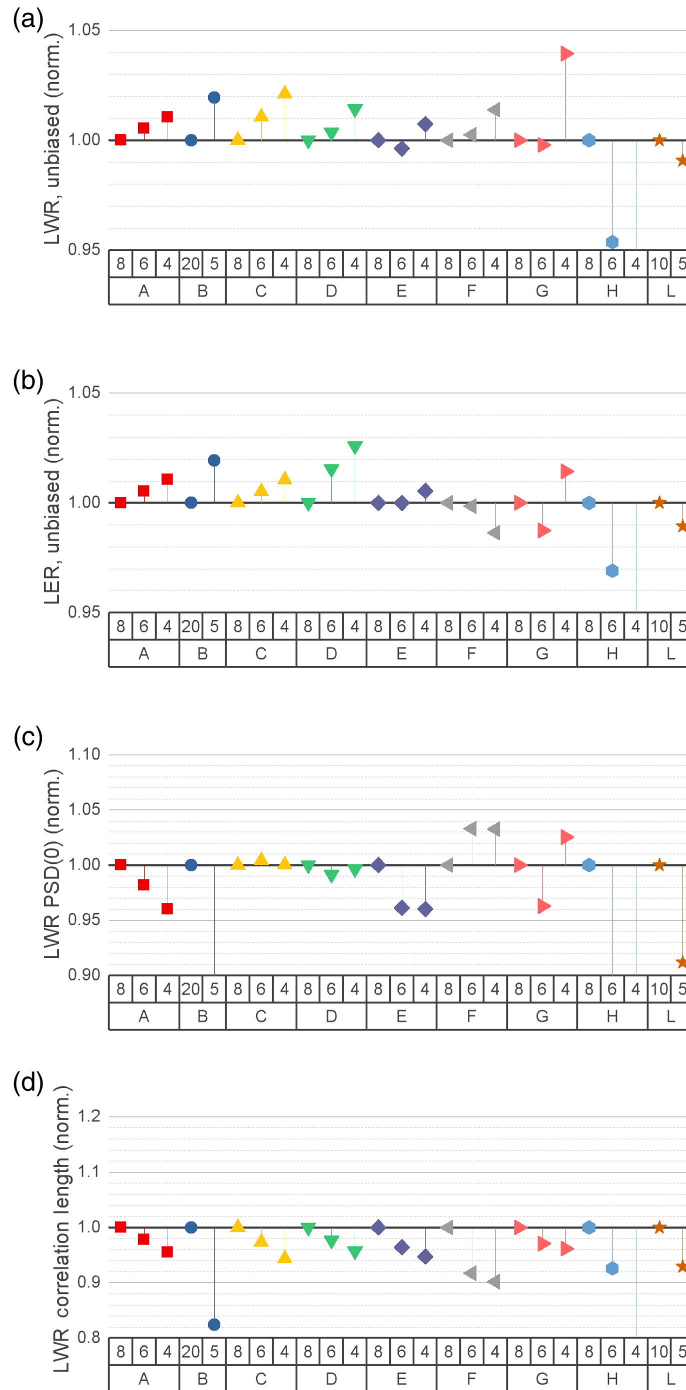

Fig. 10 (a) Total unbiased line width roughness, (b) total unbiased line edge roughness, (c) line width roughness power spectral density at zero frequency, and (d) line width roughness correlation length of a CAR patterned by EUV lithography in dense lines/spaces arrays of pitch 28 nm on nine different underlayers (A-L) of scaled thickness. Values are normalized to those of the thickest sample of each type of underlayer. The general trend indicates that total unbiased LWR increased as the underlayers got thinner (with the exception of sample H which showed poor adhesion and >8 nm unbiased roughness and for which no conclusion can be drawn). The frequency decomposition showed that the zero-frequency component had no correlation with underlayer thickness, within $\pm 5\%$ in relative terms. However, the LWR correlation length was most affected by underlayer scaling: it decreased monotonically with thickness, regardless of underlayer type.

Downloaded From: https://www.spiedigitallibrary.org/journals/Journal-of-Micro/Nanopatterning,-Materials,-and-Metrology on 25 May 2023
Terms of Use: https://www.spiedigitallibrary.org/terms-of-use

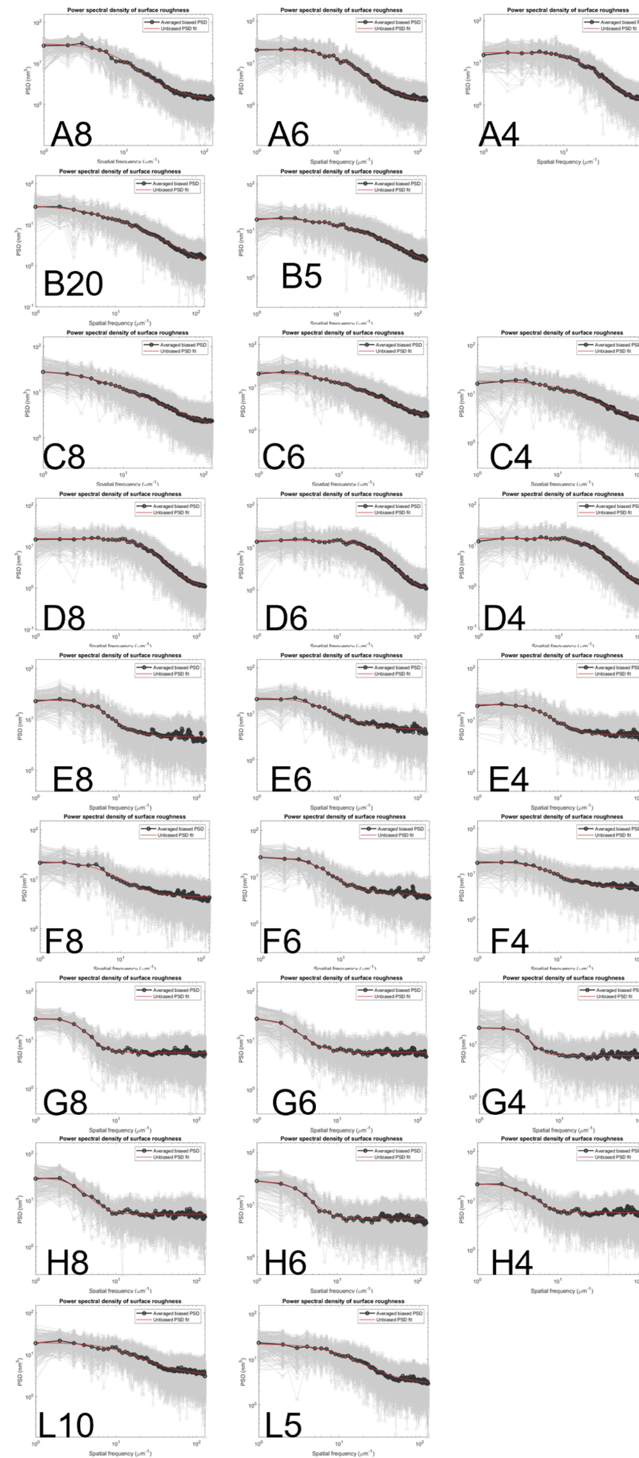

Fig. 11 Power spectral density of the surface roughness of nine underlayers of varying thickness: raw data (black symbols) and unbiased spectra (red line) calculated from raw AFM measurements. The spectra shapes vary significantly due to the nature of the films.

been caused by the decrease of correlation length of the surface roughness of the underlayers, a phenomenon widely observed in nanoscale-confined films.[16,17] To validate this hypothesis, we first calculated the power spectral densities of the blanket underlayers from AFM data and then "unbiased" the raw spectra by fitting an appropriate function as described elsewhere.[33] The PSD plots (Fig. 11) and calculated correlation lengths (Fig. 12) indicate clearly that the underlayer films are subject to a reduction in correlation length when their thickness is scaled.

Downloaded From: https://www.spiedigitallibrary.org/journals/Journal-of-Micro/Nanopatterning,-Materials,-and-Metrology on 25 May 2023
Terms of Use: https://www.spiedigitallibrary.org/terms-of-use

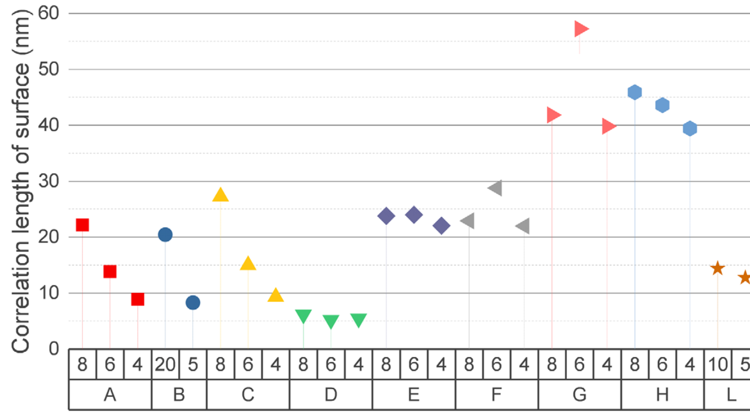

Fig. 12 The correlation length of the surface roughness of blanket underlayers was calculated from fast Fourier transform of the roughness scan data, and unbiased to remove metrology noise. Our results show a systematic reduction in correlation length of thin films when the thickness is scaled, which has consequence on the photoresist own correlation length.

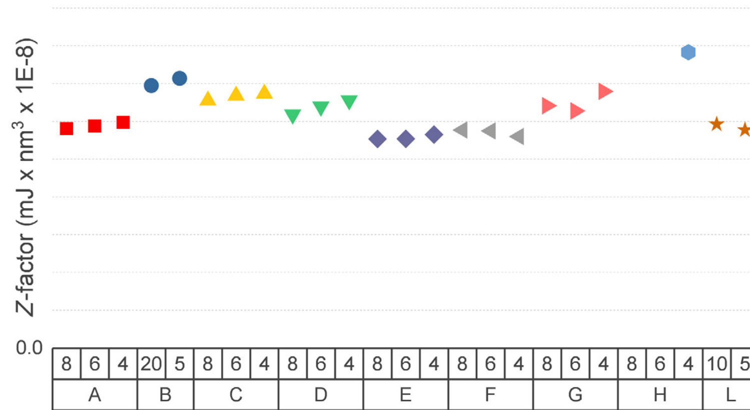

Fig. 13 *Z*-factor of CAR pitch 28 lines/spaces patterned on nine underlayers of varying thickness. Underlayer type affects *Z*-factor by as much as ±12.6%, while underlayer thickness accounts for at most ±8% variation. (Calculations do not take into account sample H due to poor adhesion.)

This observation is a novel proof that morphological features of photoresist are linked to topographic properties of underlayer at the nanoscale.

Finally, we evaluated the *Z*-factor of the same CAR patterned on the nine underlayers (Fig. 13). *Z*-factor varied by as much as ±12.6% from underlayer to underlayer, but $< \pm 8\%$ within thickness-scaled samples of the same underlayer. (Sample H is not included in the discussion.) This result shows that underlayer scaling has no detrimental effect on the CAR patterning performance, and that underlayers which perform well at 8 nm are ready for scaling down to 4 nm nominal thickness. Incidentally, it was found that the type and chemistry of underlayer have a much greater impact and can radically improve or impair photoresist performance.

4 Conclusions

Underlayers for high-NA EUV will likely be scaled down in thickness so as to meet the requirements of shallow depth of focus and etch budget. Owing to the imminent transition to high-NA EUV systems, assessment of underlayers is a technologically crucial topic, although neglected so far. In this work we studied nine underlayer types produced in thickness series, down to 4 nm nominal (~3 nm actual thickness). Materials properties (thickness, uniformity, surface roughness, and surface energy) were assessed on blanket films. The thickness and coating uniformity

Downloaded From: https://www.spiedigitallibrary.org/journals/Journal-of-Micro/Nanopatterning,-Materials,-and-Metrology on 25 May 2023
Terms of Use: https://www.spiedigitallibrary.org/terms-of-use

on 300 mm wafer-scale was satisfactory and surface energy was impacted by only a few percent in magnitude by the thickness scaling. Afterward, EUV lithography was performed using a positive tone CAR. The sensitivity, process latitude, sidewall roughness, failure-free process window, and Z-factor indicated that underlayer thickness had a very limited impact on lithography performance. Interestingly, lithography performance was more sensitive to underlayer type than thickness: in other words, when CAR performed poorly, it did so regardless of underlayer thickness which indicates that the matching between photoresist and underlayer is the major effect to look for when optimizing underlayers.

In addition, a subtle effect of underlayer thickness was detected: CAR patterned on thinner versions of the same underlayer yielded a higher-frequency component of LWR. This effect was common among all underlayers and accounted for about 5% increase in total LWR and 10% reduction in correlation length. We proved that the correlation length of surface roughness of underlayers was also decreasing when scaling thickness, an effect possibly ascribed to nanoscale confinement of thin films that eventually also impacts the correlation length of the LWR of the photoresist patterns.

In summary, state-of-the-art underlayers presented in this work are ready for scaling thickness in view of high-NA EUV lithography. These results also prove that underlayers have the greatest potential to affect the lithography process if we learn and control the correct process parameters. Understanding how the physical parameters of the underlayer impact the photoresist performance is crucial for material suppliers and lithographers. Insightful analysis requires a rigorous statistical approach to predict how physical properties of density, roughness, and surface energy (the independent variables) influence dose-to-size, exposure latitude, LWR, Z-factor, and others (the dependent variables).

Acknowledgments

The authors are grateful to materials suppliers for providing the underlayers and photoresist in the framework of joint development projects. The technical support of IMEC colleagues Nadia Vandenbroeck, Hilde Tielens, Waut Drent, and Jelle Vandereyken is also kindly acknowledged. Part of this work has been published as a proceeding of the SPIE Photomask Technology + EUV Lithography Conference 2022, Monterey CA.

References

1. C. Smeets et al., "0.33 NA EUV systems for high-volume manufacturing," *Proc. SPIE* **PC12051**, PC1205103 (2022).
2. J. Van Schoot et al., "High-NA EUV lithography exposure tool: advantages and program progress," *Proc. SPIE* **11517**, 1151712.
3. C. A. Mack, *Fundamental Principles of Optical Lithography: The Science of Microfabrication*, Wiley, Chichester, West Sussex, England; Hoboken, NJ, USA (2007).
4. M. Neisser et al., "Lithography," in *IEEE Int. Roadmap for Devices and Syst. Outbriefs*, November, Santa Clara, CA, USA, pp. 1–11 (2021).
5. A. Robinson and R. Lawson, eds., *Materials and Processes for Next Generation Lithography*, Elsevier, Amsterdam (2016).
6. D. De Simone et al., "EUV photoresist patterning characterization for imec N7/N5 technology," *Proc. SPIE* **10583**, 105830G.
7. J. Santaclara et al., "Resist and reticle activities towards High-NA EUV ecosystem readiness," *Proc. SPIE* **PC12051**, PC1205105.
8. R. Fallica et al., "Adhesion and collapse of extreme ultraviolet photoresists and the role of underlayers," *J. Micro/Nanopattern. Mater. Metrol.* **21**(3), 034601 (2022).
9. D. De Simone et al., "A lithographic and etching study on EUV contact hole patterning for stochastic process mitigation towards advanced device scaling," *Proc. SPIE* **PC12051**, PC120510P (2022).
10. G. F. Lorusso et al., "Metrology of thin resist for high NA EUVL," *Proc. SPIE* **12053**, 120530O (2022).

Downloaded From: https://www.spiedigitallibrary.org/journals/Journal-of-Micro/Nanopatterning,-Materials,-and-Metrology on 25 May 2023
Terms of Use: https://www.spiedigitallibrary.org/terms-of-use

11. C. A. Mack et al., "Unbiased roughness measurements from low signal-to-noise ratio SEM images," *Proc. SPIE* **12053**, 120530K (2022).
12. A. Raley et al., "Outlook for high-NA EUV patterning: a holistic patterning approach to address upcoming challenges," *Proc. SPIE* **12056**, 120560A (2022).
13. H. S. Suh et al., "Exploring the synergy between EUV lithography and directed self-assembly," *Proc. SPIE* **PC12054**, PC1205402 (2022).
14. C. B. Roth, "Polymers under nanoconfinement: where are we now in understanding local property changes?" *Chem. Soc. Rev.* **50**(14), 8050–8066 (2021).
15. J. M. Torres, C. M. Stafford, and B. D. Vogt, "Elastic modulus of amorphous polymer thin films: relationship to the glass transition temperature," *ACS Nano* **3**(9), 2677–2685 (2009).
16. F. Elsholz, E. Schöll, and A. Rosenfeld, "Control of surface roughness in amorphous thin-film growth," *Appl. Phys. Lett.* **84**(21), 4167–4169 (2004).
17. T. Gredig, E. A. Silverstein, and M. P. Byrne, "Height-Height correlation function to determine grain size in iron phthalocyanine thin films," *J. Phys.: Conf. Ser.* **417**, 012069 (2013).
18. Y. Han et al., "Comparing refractive index and density changes with decreasing film thickness in thin supported films across different polymers," *J. Chem. Phys.* **153**(4), 044902 (2020).
19. P. F. Green, E. Glynos, and B. Frieberg, "Polymer films of nanoscale thickness: linear chain and star-shaped macromolecular architectures," *MRS Commun.* **5**(3), 423–434 (2015).
20. M. Raible et al., "Amorphous thin-film growth: theory compared with experiment," *Europhys. Lett.* **50**(1), 61–67 (2000).
21. C. Higgins et al., "Understanding ultra-thin film resist and underlayer performance through physical characterization," *J. Photopolym. Sci. Technol.* **23**(5), 699–707 (2010).
22. J. H. Sim et al., "Thickness dependence of properties of EUV underlayer thin films," *Proc. SPIE* **12055**, 120550B (2022).
23. M. Morita et al., "Growth of native oxide on a silicon surface," *J. Appl. Phys.* **68**(3), 1272–1281 (1990).
24. C. Bohling and W. Sigmund, "Self-limitation of native oxides explained," *Silicon* **8**(3), 339–343 (2016).
25. M. Frigo and S. G. Johnson, "FFTW: an adaptive software architecture for the FFT," in *Proc. IEEE Int. Conf. Acoust., Speech and Signal Process., ICASSP '98 (Cat. No.98CH36181)*, Seattle, WA, USA, Vol. 3, pp. 1381–1384 (1998).
26. P. Vanelderen et al., "Underlayer optimization method for EUV lithography," *Proc. SPIE* **11326**, 1132615 (2020).
27. G. F. Lorusso et al., "Need for LWR metrology standardization: the imec roughness protocol," *J. Micro/Nanolith. MEMS MOEMS* **17**(4), 041009 (2018).
28. C. A. Mack and B. D. Bunday, "Analytical linescan model for SEM metrology," *Proc. SPIE* **9424**, 117–139 (2015).
29. G. P. Patsis et al., "Roughness analysis of lithographically produced nanostructures: off-line measurement and scaling analysis," *Microelectron. Eng.* **67–68**, 319–325 (2003).
30. M. Kamijo et al., "Mean-square radius of gyration of isotactic oligo- and poly(methyl methacrylate)s in dilute solution," *Macromolecules* **27**(20), 5697–5703 (1994).
31. D. Marton and J. Fine, "On the development of increasing surface roughness during ion sputtering," *Thin Solid Films* **151**(3), 433–439 (1987).
32. T. Wallow et al., "Evaluation of EUV resist materials for use at the 32 nm half-pitch node," *Proc. SPIE* **6921**, 69211F (2008).
33. G. F. Lorusso et al., "Unbiased roughness measurements: subtracting out SEM effects," *Microelectron. Eng.* **190**, 33–37 (2018).

Biographies of the authors are not available.

Downloaded From: https://www.spiedigitallibrary.org/journals/Journal-of-Micro/Nanopatterning,-Materials,-and-Metrology on 25 May 2023
Terms of Use: https://www.spiedigitallibrary.org/terms-of-use